Hindawi
Journal of Chemistry
Volume 2022, Article ID 6894049, 10 pages
https://doi.org/10.1155/2022/6894049

Research Article

Facile Synthesis of Copper-Coated-Reduced-Graphene-Oxide and Its Application as a Highly Sensitive Electrochemical Sensor for Hydroquinone

Youzhi Yao

Wuhu Institute of Technology, Wuhu 241003, China

Correspondence should be addressed to Youzhi Yao; yaoyz@whit.edu.cn

Received 19 July 2022; Revised 3 October 2022; Accepted 5 October 2022; Published 14 October 2022

Academic Editor: Liviu Mitu

A facile step-by-step approach for synthesizing copper nanoparticles (CuNPs) loaded on the wrinkled surface of reduced-graphene-oxide (Cu/rGO) was conducted using a reductant at room temperature. Multiple characterization methods were applied to specify the morphology and composition of the nanocomposites. The scanning electron microscope and transmission electron microscope of Cu/rGO show that spherical CuNps were dispersed uniformly on the surface of rGO. In addition, the characteristic peaks of Cu and carbon in energy dispersive X-ray spectroscopy and X-ray photoelectron spectroscopy analyses spectra proved that Cu/rGO nanocomposites were synthesized. Soon afterwards, a new hydroquinone electrochemical sensor was prepared with Cu/rGO and a glassy carbon electrode. The sensor was characterized by cyclic voltammetry and electrochemical impedance spectroscopy. Hydroquinone was detected by differential pulse voltammetry using the composite electrode. Under the optimal condition, the linear response range was from 0.05 μM to 90 μM; the detection limit is 0.02 μM (S/N = 3) for hydroquinone. The electrochemical sensor exhibited high sensitivity in practical environmental water sample detection.

1. Introduction

Compared with other metals, copper has attracted extensive attention because of its wide source, low cost, and rich morphology. Copper nanoparticles (CuNPs) can promote electron transfer at low overpotential and excellent electrocatalytic activity [1]. On the other hand, due to the high surface activity, CuNPs are easy to be oxidized by oxygen in the air at room temperature [2]. The catalytic activity of copper is inhibited due to the formation of an oxide layer on the surface of copper.

In order to solve the problem that CuNPs are easy to be oxidized, various copper nanocomposites have been prepared, such as Cu/polypyrrole [3], Cu/carbon nanotube [4], and Cu/reduced graphene oxide (rGO) [5]. In fact, Cu nanoparticles fixed on two-dimensional flakes or other nanomaterials can improve their vulnerability effectively [6]. Graphene is one of the best materials to prevent CuNPs from being easily oxidized at room temperature [7]. Since 2004, due to high electron transport, large surface area, high mechanical strength, and high electrocatalytic activity [8], the preparation of various composites with graphene has been widely studied, for instance, the preparation of graphene and metal nanoparticles Au/GO [9], Ag/GO [10], and Cu/GO [11–13].

With high stability, excellent conductivity, catalytic performance [14], and good electrochemical activity, Cu nanocomposites have been employed in wastewater determination and treatment [15, 16]. Various approaches have been used to prepare Cu/GO nanocomposites with different morphologies [17, 18]. For example, Cu/GO with nacre structure was prepared by molecular level mixing and the self-assembly method, and Cu/GO with multilayer structure was prepared by using the ball milling method [19]. Recently, Kappagantula et al. fabricated macroscopic Cu/GO composites with enhanced electrical properties at 450°C and nitrogen atmosphere [20].

Hydroquinone is employed extensively in coal tar production, dye synthesis, paper industry, photographic

developer, cosmetics, drugs, and so on [21]. Due to the low degradation rate in the ecological environment, HQ exists in daily necessities for a long time, affecting people's health. Hydroquinone has a strong corrosive effect on the skin and mucosa, which can inhibit the central nervous system or damage liver and skin functions. In 2017, the list of carcinogens published by the International Agency for Research on Cancer of the World Health Organization was preliminarily sorted out for reference. Hydroquinone was included in the list of three types of carcinogens. The acceptable emission in the Chinese national standard is less than 0.5 mg·mL^{-1} [22]. There are many methods for HQ detection, such as electrochemical sensors [23], gas chromatography [24], spectrophotometry [25], high-performance liquid chromatography, and fluorescence [26]. Among them, electrochemical sensors have attracted extensive attention because of their superiorities of low cost, small size and mass, fast detection speed, and high sensitivity. With the change of the environment and the progress of society, the stability and sensitivity of HQ electrochemical sensors still need to be further improved [27–29].

So far, it is still a great challenge to prepare Cu/GO nanocomposites with high conductivity and good electrocatalytic performance. It is still a meaningful problem to realize the potential of high-performance Cu/GO nanocomposites by improving the dispersion of Cu in graphene matrix. In this work, a method of synthesizing highly dispersed graphene at room temperature through a simple experimental process was explored. An electrochemical sensor was prepared using the synthesized nanocomposites. The sensor was used to detect HQ as the target of toxic pollutants. It shows the characteristics of high stability and sensitivity for HQ compared to other sensors. The determination results are satisfactory.

2. Experimental

2.1. Materials. Commercial graphite (99.9%) is provided by Beijing Jingte Carbon Technology Co., Ltd. Sodium citrate ($C_6H_5Na_3O_7$), sodium borohydride ($NaBH_4$), copper sulfate ($CuSO_4$), hydroquinone (HQ), sodium dihydrogen phosphate (NaH_2PO_4), and disodium hydrogen phosphate (Na_2HPO_4) were purchased from Shanghai Chemical Reagent Co., Ltd. Phosphate buffer solution (PBS 0.10 M) was prepared with NaH_2PO_4 and Na_2HPO_4 (pH 3.0–9.0). All chemicals were used directly without further purification.

2.2. Characterization. The scanning electron microscope (SEM) (Hitachi, s-4800) and energy dispersive X-ray spectroscopy (EDS) (GG314-JPS-9200) were used to investigate the surface morphology and elemental content distribution spectrum of nanocomposites. The transmission electron microscope (TEM) was used to characterize the microstructure of Cu/rGO nanocomposites; lattice structure and spacing of carbon and copper on the sample surface were examined by using a high resolution transmission electron microscope (HRTEM) (JEOL, JEM 2100F).

In a conventional three electrode electrochemical workstation (CHI-660E Shanghai Chenhua Co., Ltd.), the bare glassy carbon electrode and the modified glassy carbon electrode were examined as work electrodes for electrochemical research. The resistance of various working electrodes was analyzed by electrochemical impedance spectroscopy (EIS). According to the curve shape of cyclic voltammetry (CV), the peak current and its reversibility of electrode reaction were discussed.

2.3. Synthesis of Cu/rGO Nanocomposite. The purchased commercial graphene (99.9%) was prepared into water-soluble graphene oxide by using the improved Hummers method [30]. In a typical experiment, firstly, $C_6H_5Na_3O_7$ (100 μl. 0.15 M) was added into 30 ml of GO solution (3 mg/mL) in order to prevent the Cu^{2+} reduction reaction from being too fast. The diameter of the prepared copper particles cannot reach the nanometer level without $C_6H_5Na_3O_7$. Secondly, $CuSO_4$ (2 ml, 0.15 M) was added to the mixture and stirred for 30 minutes so that Cu^{2+} could be fully combined with the functional groups on the GO surface. Thirdly, under the stirring condition, newly prepared $NaBH_4$ (0.06 M) was added in the mixed solution by a drop every 5 seconds, and the total dosage was about 5 ml. According to the following reaction formula $4Cu^{2+} + BH_4^- + 8OH^- = 4Cu + BO_2^- + 6H_2O$, copper ions were converted into copper, and GO was transformed into rGO, simultaneously. Subsequently, the solution was set for 24 hours to obtain a black precipitate. After washing and centrifugation (CT14D, Shanghai, China), the obtained samples were placed in a vacuum oven at 20°C for drying. All steps were performed at room temperature, as shown in Figure 1.

2.4. Preparation of the Modified Electrode. The glassy carbon electrode (GCE) was treated with aluminum powder before the experiment, washed by ultrasonic, and dried at room temperature for standby. 2.0 mg Cu/rGO nanocomposite, 3.0 mL ethanol, and 15 μL Nafion were mixed and sonicated for 30 minutes to obtain a uniform suspension. 2.0 mg rGO was prepared into suspension under the same conditions. The as-prepared two suspensions (Cu/rGO nanocomposite, rGO) of 6 μL were coated on several polished surfaces of the GCE, respectively. At room temperature, modified working electrodes were dried naturally.

3. Results and Discussion

3.1. Surface Morphological Analysis. The morphology of the fabricated Cu/rGO nanocomposite was examined by SEM and TEM analyses (Figure 2). Figure 2(a) shows the SEM micrograph of rGO. There are obvious folds on its surface, but no other substances are attached to it. As shown Figure 2(b), it can be clearly seen that a large number of spherical particles are attached to the folded surface of graphene, indicating the distribution of massive Cu nanoparticles on rGO. Figure 2(c) shows the energy dispersive X-ray spectroscopy (EDX) spectrum of Cu/rGO. The peak values of copper and carbon are obvious, and the peak value of a small amount of oxygen may be from the silicon matrix. The TEM morphology of the Cu/rGO nanocomposite is shown in Figure 2(d), and spherical

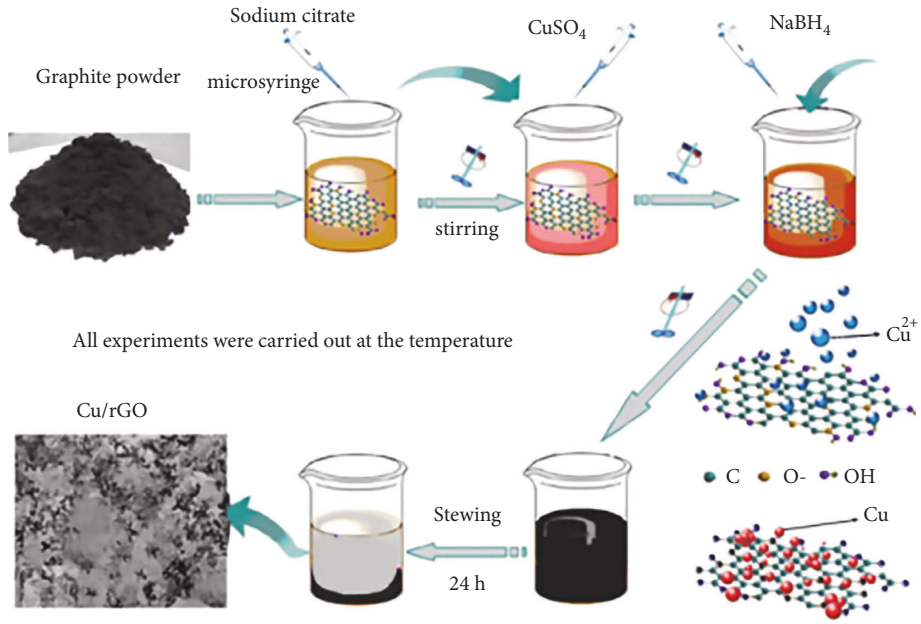

Figure 1: Schematic of the experimental setup and the growth model for Cu/rGO.

nanoparticles with uneven sizes are stacked on the surface of rGO. The HRTEM pattern of rGO is shown in Figure 2(e). The lattice spacing of two spherical copper nanoparticles measured by digital micrograph tool is approximately 0.21 nm. This finding indicates that the nanoparticles are {111} twin crystals that usually appear in fcc crystals [31]. The selected area electron diffraction (SAED) image inserted in Figure 2(d) is circular, indicating that copper on rGO is polycrystalline. The above characterization results show that Cu coated rGO nanocomposites have been synthesized successfully.

The chemical composition of the nanocomposites was analyzed using X-ray photoelectron spectroscopy (XPS). In the typical XPS spectra of GO and Cu/rGO, as shown in Figure 3(a), the peaks of C1s and O1s change significantly, especially the peak of O1s. At the same time, it can also be seen that the peak positions of C1s and O1s shift slightly, which is attributed to the different oxidation states of GO and rGO. The characteristic peak of Cu appeared at 932 eV. As shown in Figure 3(b), the peak value of C–C (sp^2 bonding in the GO) at 284.5 eV is almost unchanged, and the intensity of C–O (epoxy and acid groups) at 286.6 eV and C=O (carbonyl groups) peak at 288.4 eV is a significant decline, further indicating that GO is reduced rGO. In the Cu2p spectra (Figure 3(c)), the peaks of $Cu2p^{3/2}$ and $Cu2p^{1/2}$ appear at 932.7 and 952.5 eV, originating from metallic Cu^0. The peaks at 942.6 and 961.1 eV originate from Cu^{2+} and correspond to $Cu2p^{3/2}$ and Cu3d, respectively [32, 33]. Cu nanoparticles on the graphene surface mainly exist as Cu^0, and graphene prevents further oxidation of copper [24]. The peak at 531.8 eV in the O1s spectra could be assigned to the adsorbed oxygen species relating to –OH and H_2O or absorbed molecule O_2 (Figure 3(d)) [34].

Electrochemical impedance spectroscopy (EIS) analysis was conducted to investigate the suitable process for sensor preparation. Figure 4 presents the Nyquist plots of GCE, rGO/GCE, and Cu/rGO/GCE in phosphate buffer solution (pH = 7.0) containing 5.0 mM $K_4Fe(CN)_6$. The impedance of each modified electrode is different, indicating that the modified nanomaterials change the conductivity of the electrode. Cu/rGO exhibits higher electronic conductivity than that of bare GCE or rGO. The increase of the electron conduction rate of the modified electrode may be attributed to the network pore structure of rGO and the small size effect of copper nanoparticles. The latter facilitates faster charge transport across graphene sheet junctions, increase the specific surface area, and provide abundant active sites for catalytic reduction [35]. The EIS pattern can be fitted by the equivalent circuit shown in the inset of Figure 4. By fitting the data, the Ret of bare GCE is calculated to be 310 Ω, indicating that the interfacial electron transfer is relatively difficult. When rGO is added to the electrode surface, due to the accelerated electron transfer of rGO, the Ret value is significantly reduced to 186 Ω, and the Ret value of Cu/rGO/GCE is smaller, which is 162 Ω, indicating that the electron transfer is faster on the electrode surface modified by Cu/rGO/GCE. These results showed that rGO and Cu/rGO were successfully modified on GCE.

3.2. Electrochemical Behavior of HQ on Various Electrodes. The electrocatalytic activity of the three prepared electrochemical sensors was evaluated by CV in 0.10 M PBS (pH 7.0) containing 5.0 μM HQ at 120 $mV \cdot s^{-1}$ scanning rate, and the response spectra of the three sensors to HQ are shown in Figure 5. The redox peak of HQ appeared in all three curves, in which the peak value in the curve of Cu/rGO/GCE is maximum.

According to the Laviron formula: $Ip = nFQv/4RT$, n is calculated to be equal to 2.2, conforming to the double electron reaction formula.

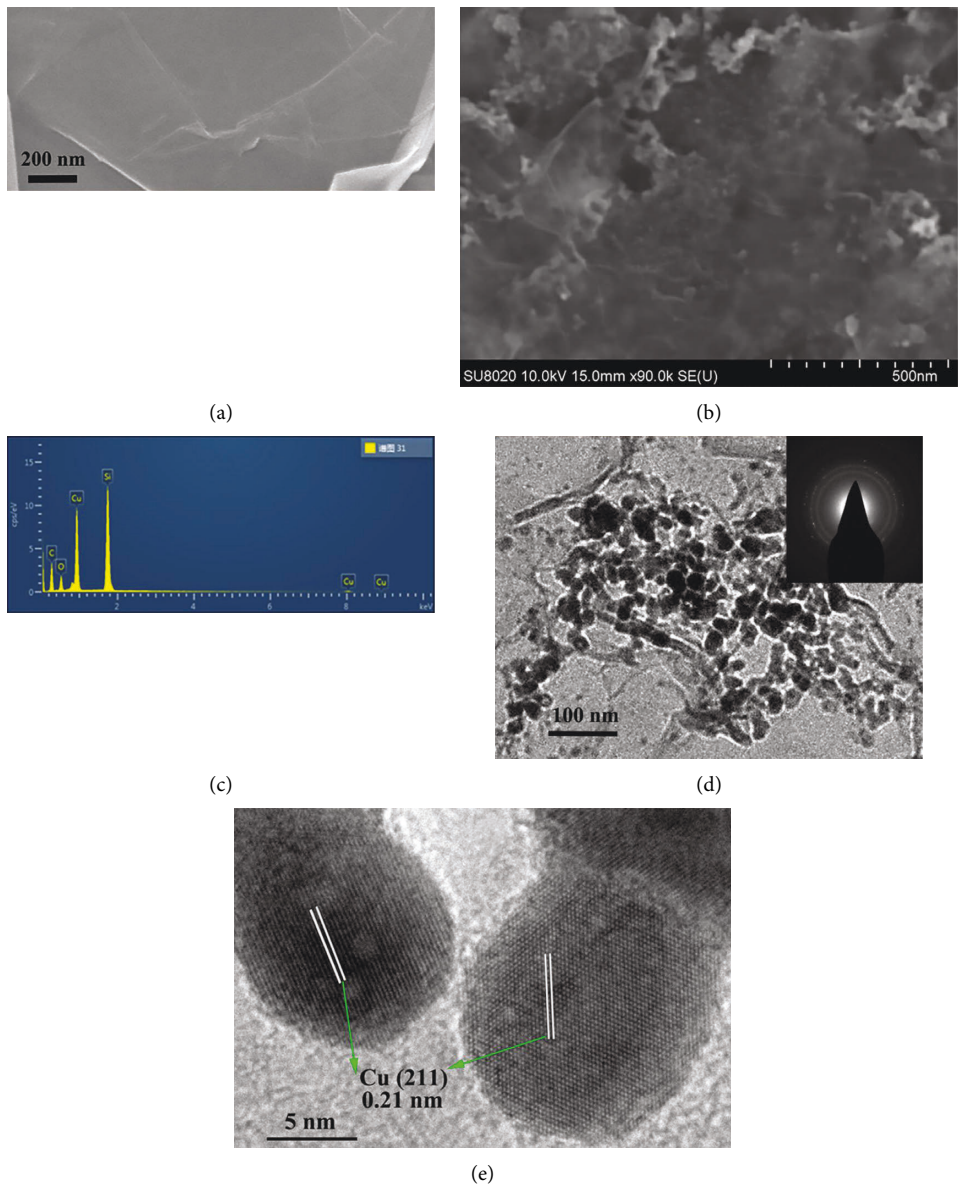

Figure 2: SEM, EDX, TEM, and HRTEM images of Cu/rGO.

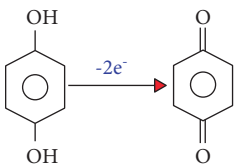

The area of the modified electrode was calculated according to the formula: $I_P = 2.69 \times 10^5\, n^{3/2}\, Acd^{1/2}\, v^{1/2}$ (Randles–Sevcik formula); the effective surface areas of the three electrodes were $A_{GCE} = 0.023\,cm^2$, $A_{rGO/GCE} = 0.032\,cm^2$, and $A_{Cu/rGO/GCE} = 0.042\,cm^2$, respectively.

The peak in the curve of Cu/rGO/GCE exhibits higher value because of the synergistic effect of Cu and rGO. In addition, the above calculation results indicate that Cu nanoparticles enhanced the effective surface area of the electron transport and the number of highly active catalytic sites [36], leading to a higher CV peak current. Thereby, Cu/rGO/GCE has the best electrocatalytic activity among the three sensors.

3.3. Optimization of Experimental Parameters for the Determination of HQ. The coating amount and acidity of Cu/rGO suspension are the key parameters affecting the performance of the modified electrode. The effect of HQ on the current of reduction peak was investigated by changing the amount of Cu/rGO suspension. As shown in Figure 6, the volume of Cu/rGO suspension coated on the surface of GCE increased from 1 μL to 6 μL. The current increased significantly, indicating that Cu/rGO increased the active area and accumulation efficiency of the GCE surface. As the volume of Cu/rGO suspension increased from 6 μL to 10 μL, the peak

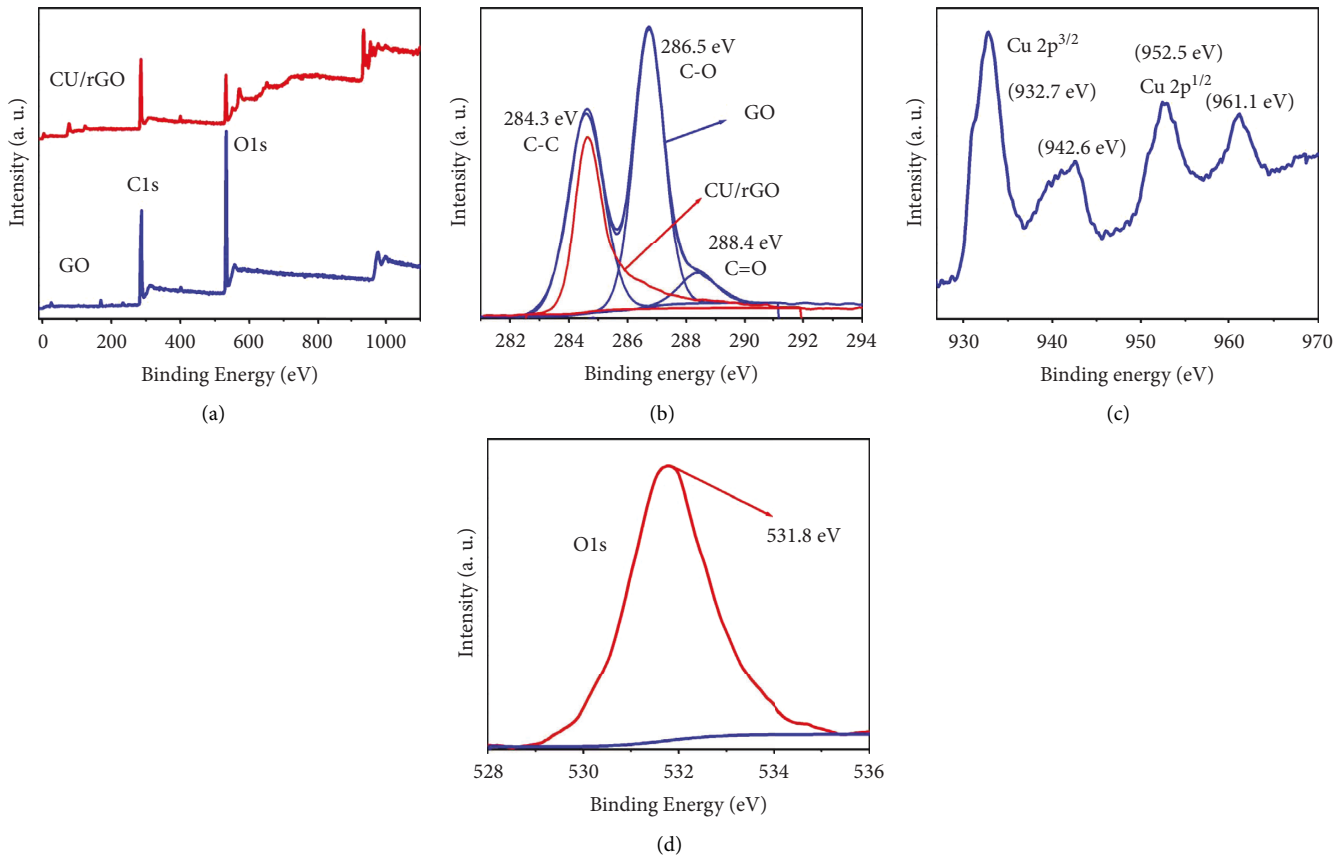

Figure 3: XPS spectra of GO and Cu/rGO: (a) survey; (b) C1s; (c) Cu 2p; (d) O1s.

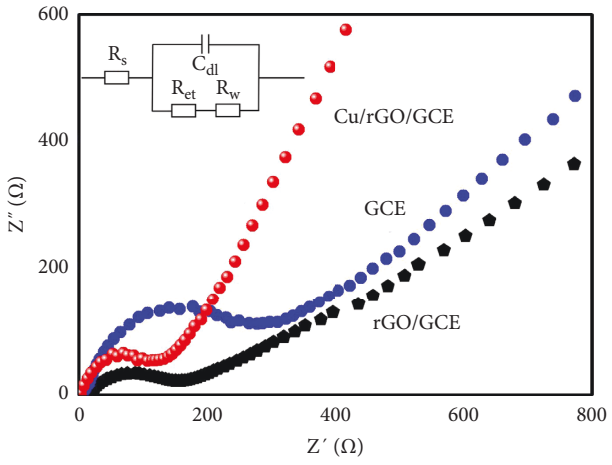

Figure 4: Nyquist plots of GCE, rGO/GCE, and Cu/rGO/GCE in 1.0 mM $[Fe(CN)_6]^{3-/4-}$ solution, inset: equivalent circuit.

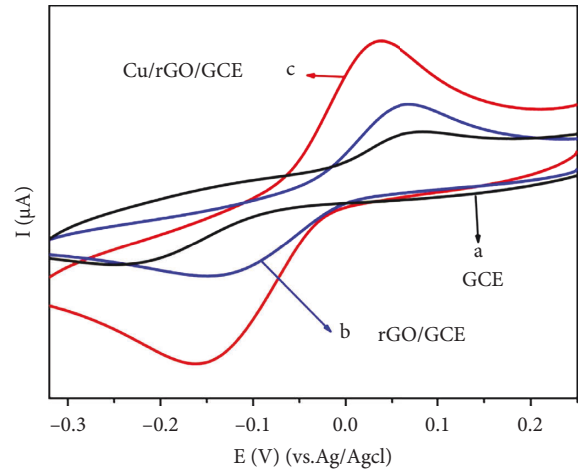

Figure 5: CV of GCE (a), rGO/GCE (b), and Cu/rGO/GCE (c) in PBS containing 5.0 μM HQ; scanning rate, 120 mV·s^{-1}.

current decreased gradually. This result may be due to the thick Cu/rGO film hindering the conductivity [37]. Therefore, the surface of GCE modified by 6 μL Cu/rGO suspension was appropriate to achieve the highest sensitivity.

According to $C_6H_4(OH)_2 - 2e^- = C_6H_4O_2 + 2H^+$, protons participate in the electrode reaction. Therefore, the peak current generated by HQ electrochemical process will change significantly under different acidities. The effect of pH on HQ oxidation was studied carefully by CV in the acidity range of pH 3.0–9.0 with Cu/rGO/GCE. As shown in Figure 7(a), the anodic peak potential of HQ shifts negatively with the increase of pH value from 3.0 to 9.0, indicating that protons are involved directly in the electrochemical redox process. The linear equation between E_{pa} and pH is $E_{pa}(V) = -0.05712\text{pH} + 0.4206$ ($R = 0.9986$), and the slope of HQ is 57.26 mV·pH^{-1}, which is close to the theoretical value of 59.0 mV·pH^{-1}, indicating that the electrochemical

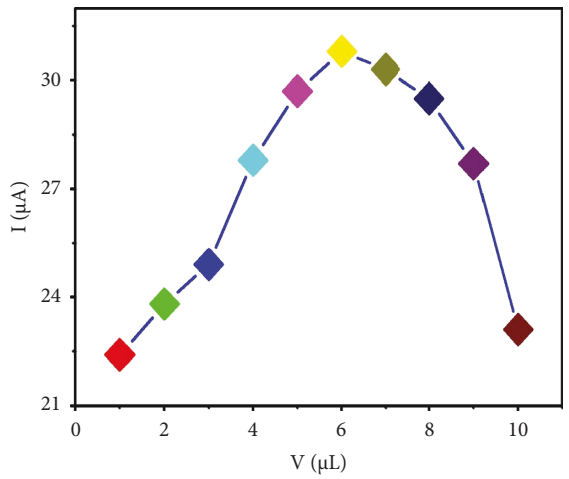

Figure 6: Effect of the amount of Cu/rGO suspension on the current of reduction peak (5.0 μM HQ at 120 mV·s^{-1} scanning rate).

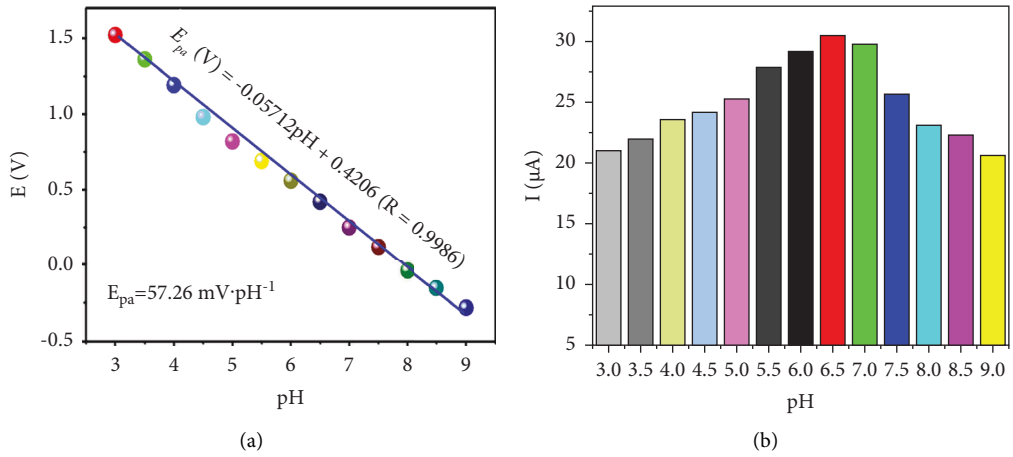

Figure 7: (a) The relationship between pH and the peak potentials. (b) The relationship between pH and the peak currents of HQ (5.0 μM HQ at 120 mV·s^{-1} scanning rate).

redox process of HQ with equal proton and electron numbers has taken place on the electrode surface [38].

As can be seen from Figure 7(b), the peak current of HQ oxidation increases with the increase of pH value from 3.0 to 6.5, while when the pH value is higher than 6.5, the peak current decreases. The possible reason is that the pKa value is 9.85. With the increase of pH value, the protonated aromatic isomer is easy to deproton and transform into an anion. The surface of Cu/rGO/GCE is negatively charged, the electrostatic repulsion between them is enhanced, and the adsorption amount of isomer on the electrode surface is reduced, resulting in the decrease of current peak value [39]. Considering the measurement sensitivity, the electrolyte with a pH value of 6.5 was selected as the best experimental condition for subsequent detection of HQ.

In order to study the kinetic reaction of the electrode/electrolyte, the influence of the scanning rate on the electrochemical behavior was examined in 0.1 M PBS solution containing 5.0 μM HQ to obtain the optimized Cu/rGO/GCE by CV. As shown in Figure 8, with a change in the scanning rate from 10 to 240 mVs^{-1}, the peak current of the cathode and anode increases accordingly. It can also be seen

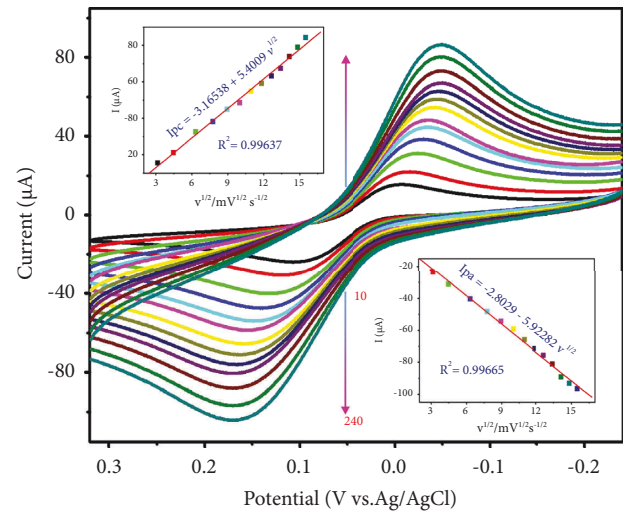

Figure 8: Cyclic voltammograms at Cu/rGO/GCE in 0.1 M PBS (pH 6.5) containing 5.0 μM HQ with different scan rates of 10, 20, 40, 60, 80, 100, 120, 150, 180, 200, 220, and 240 mV·s^{-1}, respectively. Plots of peak currents vs. the square root of scan rates for HQ (inset).

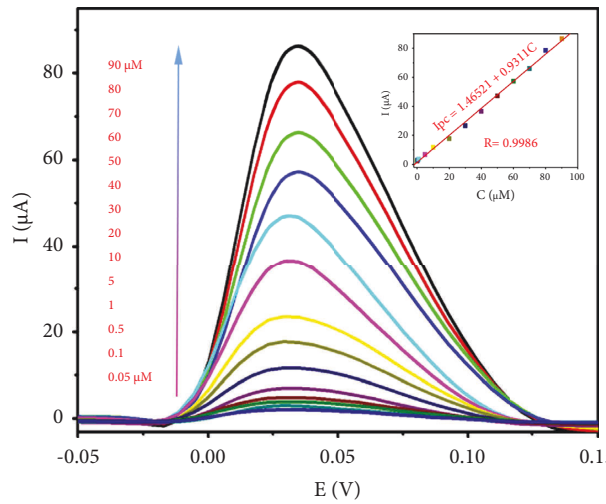

Figure 9: DPV curves of different concentrations of HQ (0.05–90 μM) at Cu/rGO/GCE in 0.10 M PBS (pH 6.5). The insert shows the relationship between peak current and concentration of HQ.

Table 1: A comparison of the reported electrochemical sensors for hydroquinone.

Electrode	Technique	Linear range (μM)	Lod (μM)	Ref.
Zn@ZnO	Cyclic voltammetry	10–90	0.10443	[27]
Nano-co/poly-L-glu	Cyclic voltammetry	3.58–130	0.497	[21]
Polypyrrole/carbon black/ZnO	Amp	0.9–6.5	0.0229	[40]
AuNPs/EGP	DPV	0.07–100	0.0273	[41]
TiO_2–ZnO-rGO	DPV	0.1–500	0.031	[42]
Cu/RGO	DPV	0.05–86.5	0.02	This work

that the peak potential of anodic oxidation (E_{pc}) and cathodic reduction (E_{pa}) moves slightly to the positive potential and negative potential, respectively, indicating that the electrochemical reaction process is a quasireversible process. Generally speaking, the potential change observed is attributed to the corresponding change of catalytic point reaction activity on the material surface with the change of the scanning rate.

The value of Ipc, Ipa, and the square root of the scanning rate in the range of 10 to 240 mVs-1 scanning rate (v 1/2) is linear, as shown in the insertion diagram of Figure 8, which can be described by the following linear regression equation:

$$\begin{aligned} I_{pc} &= -3.16538 + 5.4009v^{1/2}, \quad R^2 = 0.99637, \\ I_{pa} &= -2.8029 + 5.922802v^{1/2}, \quad R^2 = 0.99665. \end{aligned} \tag{1}$$

Therefore, the electrochemical sensing of HQ is a diffusion-controlled process.

3.4. Determination of HQ. Under the optimum experimental conditions, HQ on Cu/rGO/GCE was determined quantitatively by differential pulse voltammetry (DPV) because it has high current sensitivity and good resolution. As shown in Figure 9, there is a good linear relationship between the oxidation peak current of HQ and its concentration. When the concentrations of HQ were in the range of 0.05 μM to 90 μM, as shown in the inset of Figure 9, the linear regression equation is $I_{pc} = 1.46521 + 0.9311C$, $R = 0.9986$; the detection limit for HQ is estimated to be 0.02 μM (S/N = 3).

The results of HQ determination with different modified electrodes were also compared. The linear detection limits and ranges are shown in Table 1. The results show that the linear range of HQ is wide, and the detection limit is lower than that of most published papers. Therefore, compared with other modified electrodes, Cu/rGO/GCE is a competitive candidate electrochemical sensor for HQ determination.

3.5. Reproducibility, Repeatability, Stability, and Selectivity. The electrochemical performance of the prepared sensor in solution containing 5.0 μM HQ was assessed to evaluate the reproducibility of Cu/rGO/GCE. Five independently fabricated electrodes exhibited similar responses, with a relative standard deviation (RSD) of 3.2%. The repeatability of the sensors was examined by continuous measurements using the same concentration of HQ (5.0 μM). The sensor exhibited good reproducibility (2.3% RSD) after 10 repeated measurements. These results indicate the excellent stability and repeatability of the sensors. The sensors based on Cu/rGO/GCE were stored in a constant temperature drying oven when they were not used. As seen in Figure 10(a), after 30 days of segmented testing, the current response to HQ decreases to 95.18%, indicating that Cu/rGO/GCE exhibits good stability.

As shown in Figure 10(b), the selectivity of the sensor was evaluated through DPV by adding some potential interfering compounds including phenol, resorcin, catechol, glucose, and

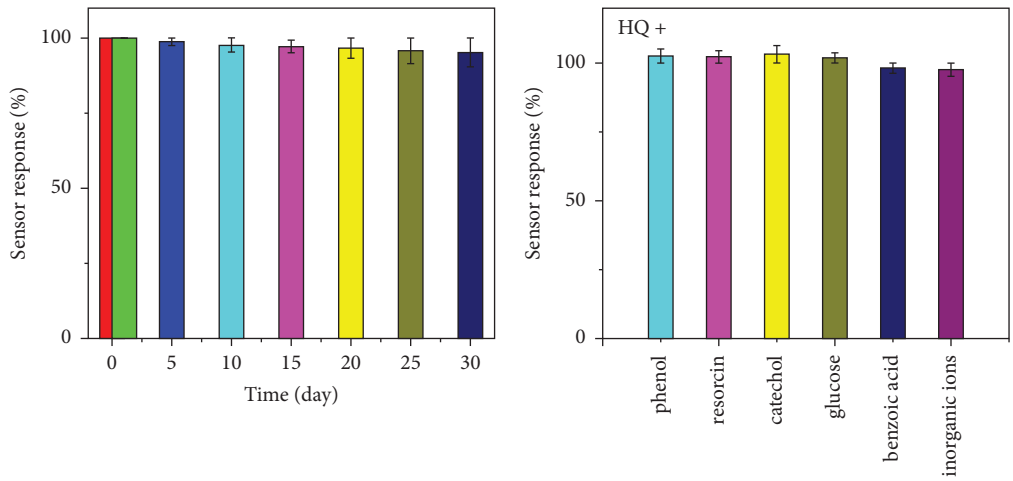

Figure 10: (a) Storage stability of Cu/rGO/GCE stored in a constant temperature drying oven, (b) the selectivity of the proposed method for HQ determination. The concentration of HQ is 5 μM, concentrations of phenol, resorcin, catechol, glucose, and benzoic acid are 0.5 mM, concentration of inorganic ions is 1 mM; the error bars illustrate the standard deviations of six independent measurements.

Table 2: Determination results for HQ in local tap and reservoir water.

Samples	Serial number	Added (μM)	Found (nM)	Recovery (%)	RSD (%)	Found (nM)	Recovery (%)	RSD (%)
		Cu/rGO/GCE sensor				HPLC-UV		
Tap water	1	10.0	9.8	98.0	3.2	9.9	99.0	4.1
	2	20.0	19.7	98.5	2.3	19.8	97.5	3.2
	3	30.0	30.5	101.7	4.1	30.2	100.7	3.6
Reservoir water	1	10.0	10.2	102.0	4.2	9.7	97.0	2.8
	2	20.0	19.4	97.0	3.9	19.6	98.0	3.5
	3	30.0	29.6	98.7	2.5	29.5	98.3	2.7

benzoic acid in HQ solution. In the presence of these interfering substances, no obvious current response was detected. Some inorganic ions (Na^+, Ca^{2+}, Fe^{3+}, Zn^{2+}, Cu^{2+}, Cl^-, CO_3^{2-}, and NO_3^-) were also added in the solution. These ions also did not interfere significantly with the detection process.

3.6. Sample Analysis. The Cu/rGO/GCE was applied to determine HQ in practical water samples (local tap water and water from a local reservoir). Based on DPV analysis, target analytes were not found in the water samples, indicating that the concentration of HQ may be lower than the detection limits. Therefore, the standard addition technique was performed by adding known concentrations of HQ prior to analysis. The experimental results are listed in Table 2. The recoveries of the samples are within 97.0%–102.0% for HQ, which is in good agreement with the real addition. The RSD values are less than 5%, which is acceptable.

The same samples were also determined by using the HPLC-UV technique. It can be seen from the table, the data obtained by the two methods are almost identical, which indicates that the method of determining HQ by using the Cu/rGO/GCE sensor is reliable. The Cu/rGO/GCE sensor can be efficiently used to determine HQ in real samples.

It is an average value of eight measurements.

4. Conclusions

This work describes a facile method for preparation of Cu/rGO at the temperature. The novel nanocomposite was used to develop a new electrochemical sensor for simple, sensitive, and stable determination of HQ. The electrochemical activity of the modified electrode can be greatly improved by combining Cu nanoparticles immobilized on rGO. The fabricated Cu/rGO/GCE was applied for HQ detection and showed wide linear range and low detection limit. The proposed sensor was also applied for real-sample detection of HQ, and satisfactory results were obtained. Overall, the proposed potential platform can be applied for simple and effective detection of HQ.

Data Availability

Data are available on request from the authors.

Conflicts of Interest

The author declares that there are no conflicts of interest.

Acknowledgments

The authors gratefully acknowledge the financial support from the Wuhu Institute of Technology (Kjcxpt202004,

rc2021dtr06). The authors also thank Professor, Ph.D. supervisor Zhousheng Yang, Professor Kunhong Hu, and Dr. Jun Liu for their assistance. Wuhu Engineering Technology Research Center of environmental monitoring and Control: Kjcxpt202004 Academic and technical leader: rc2021dtr06.

References

[1] S. Pourbeyram, J. Abdollahpour, and M. Soltanpour, "Green synthesis of copper oxide nanoparticles decorated reduced graphene oxide for high sensitive detection of glucose," *Materials Science and Engineering: C*, vol. 94, pp. 850–857, 2019.

[2] D. M. Ye, G. Z. La, G. G. Wang et al., "One-pot synthesis of copper nanowire decorated by reduced graphene oxide with excellent oxidation resistance and stability," *Applied Surface Science*, vol. 467, no. 468, pp. 158–167, 2019.

[3] K. Liu, Y. H. Li, H. Y. Zhang, and Y. C. Liu, "Synthesis of the polypyrrole encapsulated copper nanowires with excellent oxidation resistance and temporal stability," *Applied Surface Science*, vol. 439, pp. 226–231, 2018.

[4] H. Z. Guo, J. R. Jin, Y. Z. Chen et al., "Controllable synthesis of Cu-Ni core-shell nanoparticles and nanowires with tunable magnetic properties," *Chemical Communications*, vol. 52, no. 42, pp. 6918–6921, 2016.

[5] S. Huang, Q. Zhang, P. Li, F. Ren, A. Yurtsever, and D. Ma, "High-performance suspended particle devices based on copper-reduced graphene oxide core-shell nanowire electrodes," *Advanced Energy Materials*, vol. 8, no. 18, Article ID 1703658, 2018.

[6] A. Aliprandi, T. Moreira, C. Anichini et al., "Hybrid copper nanowire reduced graphene oxide coatings: a green solution toward highly transparent, highly conductive, and flexible electrodes for (opto) electronics," *Advanced Materials*, vol. 29, no. 41, Article ID 1703225, 2017.

[7] R. Jakhar, J. E. Yap, and R. Joshi, "Microwave reduction of graphene oxide," *Carbon*, vol. 170, pp. 277–293, 2020.

[8] S. J. Rowley-Neale, E. P. Randviir, A. S. Abo Dena, and C. E. Banks, "An overview of recent applications of reduced graphene oxide as a basis of electroanalytical sensing platforms," *Applied Materials Today*, vol. 10, pp. 218–226, 2018.

[9] I. Cesarino, R. P. Simões, F. C. Lavarda, and A. Batagin-Neto, "Electrochemical oxidation of sulfamethazine on a glassy carbon electrode modified with graphene and gold nanoparticles," *Electrochimica Acta*, vol. 192, pp. 8–14, 2016.

[10] D. L. C. Golinelli, S. A. S. Machado, and I. Cesarino, "Synthesis of silver nanoparticle-graphene composites for electroanalysis applications using chemical and electrochemical methods," *Electroanalysis*, vol. 29, no. 4, pp. 1014–1021, 2016.

[11] M. K. L. Da Silva, R. Plana Simões, and I. Cesarino, "Evaluation of reduced graphene oxide modified with antimony and copper nanoparticles for levofloxacin oxidation," *Electroanalysis*, vol. 30, no. 9, pp. 2066–2076, 2018.

[12] D. Shin, S. J. Choi, S. Eunkyung Kim, C. S. Yun, Y. Yee Tan, and C. Sunyong Lee, "Fabrication of multilayer graphene-coated copper nanoparticles for application as a thermal interface material," *Applied Surface Science*, vol. 583, Article ID 152488, 2022.

[13] M. Z. H. Khan, M. A. Rahman, P. Yasmin et al., "Formation and characterization of copper nanocube-decorated reduced graphene oxide film," *Journal Of Nanomaterials*, vol. 6, Article ID 5702838, 2017.

[14] N. K. Ojha, G. V. Zyryanov, A. Majee, V. N. Charushin, O. N. Chupakhin, and S. Santra, "Copper nanoparticles as inexpensive and efficient catalyst: a valuable contribution in organic synthesis," *Coordination Chemistry Reviews*, vol. 353, pp. 1–57, 2017.

[15] T. Ameh and C. M. Sayes, "The potential exposure and hazards of copper nanoparticles: a review," *Environmental Toxicology and Pharmacology*, vol. 71, Article ID 103220, 2019.

[16] V. Q. Fernandes, M. K. L. Silva, and I. Cesarino, "Determination of isotretinoin (13-cis-retinoic acid) using a sensor based on reduced graphene oxide modified with copper nanoparticles," *Journal of Electroanalytical Chemistry*, vol. 856, Article ID 113692, 2020.

[17] G. Malandrino, G. G. Condorelli, G. Lanza, I. L. Fragalà, U. Scotti Di Uccio, and M. Valentino, "Effect of Ba-Ca-Cu precursor matrix on the formation and properties of superconducting Tl2Ba2Can-1CunOx films: a combined metal-organic chemical vapour deposition and thallium vapour diffusion approach," *Journal of Alloys and Compounds*, vol. 251, no. 1-2, pp. 332–336, 1997.

[18] Q. Wang, Q. Wang, M. Li, S. Szunerits, and R. Boukherroub, "Preparation of reduced graphene oxide/Cu nanoparticle composites through electrophoretic deposition: application for nonenzymatic glucose sensing," *RSC Advances*, vol. 5, no. 21, pp. 15861–15869, 2015.

[19] Z. Yang, L. Wang, Z. Shi et al., "Preparation mechanism of hierarchical layered structure of graphene/copper composite with ultrahigh tensile strength," *Carbon*, vol. 127, pp. 329–339, 2018.

[20] K. S. Kappagantula, J. A. Smith, A. K. Nittala, and F. F. Kraft, "Macro copper-graphene composites with enhanced electrical conductivity," *Journal of Alloys and Compounds*, vol. 894, Article ID 162477, 2022.

[21] B. M. Huang, C. W. Yao, J. Yang, S. Z. Du, and X. Q. Lu, "A study on the electrochemical behavior of hydroquinone at a nanometer cobalt/L-glutamate modified electrode," *RSC Advances*, vol. 10, no. 71, pp. 43834–43839, 2020.

[22] K. Karuppasamy, I. Rabani, D. Vikraman et al., "ZIF-8 templated assembly of $La3^{+}$-anchored ZnO distorted nanohexagons as an efficient active photocatalyst for the detoxification of rhodamine B in water," *Environmental Pollution*, vol. 272, Article ID 116018, 2021.

[23] Y. Z. Yao, Y. C. Liu, and Z. S. Yang, "A novel electrochemical sensor based on a glassy carbon electrode modified with Cu-MWCNT nanocomposites for determination of hydroquinone," *Analytical Methods*, vol. 8, no. 12, pp. 2568–2575, 2016.

[24] S. C. Moldoveanu and M. Kiser, "Gas chromatography/mass spectrometry versus liquid chromatography/fluorescence detection in the analysis of phenols in mainstream cigarette smoke," *Journal of Chromatography A*, vol. 1141, no. 1, pp. 90–97, 2007.

[25] P. Nagaraja, R. A. Vasantha, and K. R. Sunitha, "A sensitive and selective spectrophotometric estimation of catechol derivatives in pharmaceutical preparations," *Talanta*, vol. 55, no. 6, pp. 1039–1046, 2001.

[26] W. Gao and C. Legido-Quigley, "Fast and sensitive high performance liquid chromatography analysis of cosmetic creams for hydroquinone, phenol and six preservatives," *Journal of Chromatography A*, vol. 1218, no. 28, pp. 4307–4311, 2011.

[27] J. Park, J. Kim, A. Min, and M. Y. Choi, "Fabrication of nonenzymatic electrochemical sensor based on Zn@ZnO core-shell structures obtained via pulsed laser ablation for selective determination of hydroquinone," *Environmental Research*, vol. 204, Article ID 112340, 2022.

[28] C. X. Wang, P. C. Zhao, L. Zhang et al., "Switched electrochemical sensor for hydroquinone based on rGO@Au,

monoclinic BiVO4 and temperature-sensitive polymer composite material," *Microchemical Journal*, vol. 179, Article ID 107412, 2022.

[29] M. S. Vishwanath, B. K. Swamy, and K. A. Vishnumurthy, "Electrochemical detection of bisphenol A in presence of catechol and hydroquinone at copper oxide modified carbon paste electrode," *Materials Chemistry and Physics*, vol. 289, Article ID 126443, 2022.

[30] W. S. Hummers and R. E. Offeman, "Preparation of graphitic oxide," *Journal of the American Chemical Society*, vol. 80, no. 6, p. 1339, 1958.

[31] S. L. Wang, X. L. Huang, Y. H. He et al., "Synthesis, growth mechanism and thermal stability of copper nanoparticles encapsulated by multi-layer graphene," *Carbon*, vol. 50, no. 6, pp. 2119–2125, 2012.

[32] M. C. Biesinger, L. W. M. Lau, A. R. Gerson, and R. S. C. Smart, "Resolving surface chemical states in XPS analysis of first row transition metals, oxides and hydroxides: Sc, Ti, V, Cu and Zn," *Applied Surface Science*, vol. 257, no. 3, pp. 887–898, 2010.

[33] C. K. Wu, M. Yin, S. O'Brien, and J. T. Koberstein, "Quantitative analysis of copper oxide nanoparticle composition and structure by X-ray photoelectron spectroscopy," *Chemistry of Materials*, vol. 18, no. 25, pp. 6054–6058, 2006.

[34] Y. Hou, J. Li, Z. Wen, S. Cui, C. Yuan, and J. Chen, "Co_3O_4 nanoparticles embedded in nitrogen-doped porous carbon dodecahedrons with enhanced electrochemical properties for lithium storage and water splitting," *Nano Energy*, vol. 12, pp. 1–8, 2015.

[35] Y. Tingting, L. Ruiyi, L. Xiaohuan et al., "Nitrogen and sulphur-functionalized multiple graphene aerogel for supercapacitors with excellent electrochemical performance," *Electrochimica Acta*, vol. 187, pp. 143–152, 2016.

[36] V. Mani, R. Devasenathipathy, S. M. Chen, S. F. Wang, P. Devi, and Y. Tai, "Electrodeposition of copper nanoparticles using pectin scaffold at graphene nanosheets for electrochemical sensing of glucose and hydrogen peroxide," *Electrochimica Acta*, vol. 176, pp. 804–810, 2015.

[37] K. J. Huang, L. Wang, J. Li, M. Yu, and Y. M. Liu, "Electrochemical sensing of catechol using a glassy carbon electrode modified with a composite made from silver nanoparticles, polydopamine, and graphene," *Microchimica Acta*, vol. 180, no. 9-10, pp. 751–757, 2013.

[38] J. Zhou, X. Li, L. L. Yang et al., "The Cu-MOF-199/single-walled carbon nanotubes modified electrode for simultaneous determination of hydroquinone and catechol with extended linear ranges and lower detection limits," *Analytica Chimica Acta*, vol. 899, pp. 57–65, 2015.

[39] D. Song, J. Xia, F. Zhang et al., "Multiwall carbon nanotubes-poly (diallyldimethylammonium chloride)-graphene hybrid composite film for simultaneous determination of catechol and hydroquinone," *Sensors and Actuators B: Chemical*, vol. 206, pp. 111–118, 2015.

[40] J. Ahmed, M. Faisal, M. Jalalah, S. A. Alsareii, and F. A. Harraz, "Novel polypyrrolecarbon black doped ZnO nanocomposite for efficient amperometric detection of hydroquinone," *Journal of Electroanalytical Chemistry*, vol. 898, Article ID 115631, 2021.

[41] L. M. Fan, X. Y. Li, and X. W. Kan, "Disposable graphite paper based sensor for sensitive simultaneous determination of hydroquinone and catechol," *Electrochimica Acta*, vol. 213, pp. 504–511, 2016.

[42] X. Y. Lu, S. F. Zhang, F. Y. Kong et al., "Facile synthesis of TiO2-ZnO-rGO nanocomposites for highly sensitive simultaneous determination of hydroquinone and catechol," *Microchemical Journal*, vol. 166, Article ID 106246, 2021.